Hole scavenging and electron-hole pair production rate: two mandatory key factors to control single-tip Au-CdSe/CdS nanoheterodimers growth by photodeposition

Junjie Hao, Haochen Liu, Kai Wang, Xiao Wei Sun, Jean-Pierre Delville, Marie-Hélène Delville

Hole Scavenging and Electron-Hole Pair Production Rate: Two Mandatory Key Factors to Control Single-Tip Au-CdSe/CdS Nanoheterodimers Growth by Photodeposition

Junjie Hao[1,2], Haochen Liu[3], Kai Wang[3], Xiao Wei Sun[3], Jean-Pierre Delville[2] and Marie-Helene Delville[1*]*

[1] CNRS, Univ. Bordeaux, Bordeaux INP, ICMCB, UMR 5026, 87 avenue du Dr. A. Schweitzer, Pessac, F-33608, France.

[2] Univ. Bordeaux, CNRS, LOMA, UMR 5798, 33405 Talence, France.

[3] Department of Electrical and Electronic Engineering, Southern University of Science and Technology, Shenzhen, 518055, China.

ABSTRACT.

Metal/semiconductor heteronanostructures are now considered as benchmark functional nanomaterials for many light-driven applications. Using laser-driven photodeposition to control growth of gold nanodots (NDs) onto CdSe/CdS dot-in-rods (DRs), we show that the addition of a dedicated hole scavenger (MeOH) is *the* cornerstone to significantly reduce to less than 3.5% the multiple-site nucleation and 2.5% the rate of gold-free DRs. This means, from a synthetic point of view, that rates up to 90% of single-tip DRs can be reproducibly achieved. Moreover, by systematically varying this hole scavenger concentration and the Au/DRs ratio on the one hand, and the irradiation intensity and the time exposure on the other hand, we explain how gold deposition switches from multi-site to single-tipped, and how the growth and final size of the single photodeposited ND can be controlled. A model also establishes that the results obtained based on these different varying conditions, can be merged onto a single 'master behavior' that summarizes and predicts the single-tip gold ND growth onto the CdSe/CdS DRs. We eventually use data from the literature on growth of platinum NDs onto CdS nanorods by laser-deposition to extend our investigation to another metal of major interest and strengthen our modelling of single metallic ND growth onto II-VI semiconducting nanoparticles. This demonstrated strategy can raise a common methodology in the synthesis of single-tip semiconductor-metal hybrid nanoheterodimers (NHDs), leading to advanced nanoparticles architectures for applications in areas as different as photocatalysis, hydrogen production, photovoltaics, and light detection.

KEYWORDS. photodeposition, laser, heteronanodimers, CdSe/CdS, single tip gold nanodots, hole scavenger.

INTRODUCTION

The synergistic optical properties of metal-semiconductor hybrid nanoheterodimers (NHDs) give rise to light-induced charge separation,[1] and make them suitable for use as photocatalysts in redox reactions, including hydrogen production by water splitting,[2-7] generation of radicals and photo-degradation of organic contaminants.[8] Among the methods used to synthesize metal-semiconductor NHDs based on CdSe/CdS dot-in-rods (DRs), the most cited are the chemical reduction,[3, 9-12] the physical vapor deposition,[13-14] the impregnation-deposition[14-16] and the photodeposition.[10, 17-21] The last two decades have shown that chemical reduction [22-23] and photodeposition[19, 24-25] are likely the most efficient ones to look at the selective growth of small Au crystals at the tips of CdSe and CdS rod-shaped nanocrystals. Due to their high catalytic performance, metal-tipped seeded rod samples, such as CdSe/CdS DRs,[4, 11, 19, 21, 26-27] indeed enable an efficient long-lasting charge carrier separation and minimize the intermediates back reactions.[11] Furthermore, Amirav's group found that a catalyst semiconductor rod decorated with a single-tip (ST) metal revealed to be the most active for the hydrogen production (27 times higher than the DRs covered with multiple dots),[4, 21] and that optimizing the size of this single metallic nanocrystal does even increase catalysis efficiencies.[28] However, up to now, the detailed study of the ST NHDs photodeposition process is still rather limited especially in terms of growth mechanism.[29]

Most of the research concerning single-tip NHDs has been performed under the following conditions: low temperature,[26, 30] long alkyl amine ligands,[26] anaerobic conditions[23] or/and high reactivity gold precursors ($AuCl_3$,[26] AuCl[12]), all of them mainly set to reduce the defect deposition, thereby improving the ratio of single-tip NHDs. Moreover, even if the presence of a hole scavenger has been shown to play a vital role in the photodeposition process of semiconductors (such as TiO_2),[31-35] it has rarely been mentioned as such in the photodeposition on cadmium chalcogenide

semiconductor.[19, 25, 36-37] This is probably linked to the fact that even without the presence of a dedicated hole scavenger, the chalcogenide anions forming the rods participate to the reduction of Au^{3+} ions with a concomitant etching of the rods,[38-39] or di-dodecyl dimethyl ammonium bromide (DDAB) and dodecylamine (DDA) a primary amine claimed to act not only as a reducing and stabilizing agent, but most probably also as a hole scavenger.[37, 39-40] We should also mention that Kalisman *et al.* commented on the necessary presence of a hole scavenger to favor the hydrogen yield during the photocatalytic reaction.[21] Moreover, as far as we are aware, there is still no methodical research on the various parameters affecting the single-tip production, especially concerning the systematic variation of the ratios of single-tip (ST), double-tip (DT) and multiple-site (MS) hybrid nanoparticles (HNPs) even if the sites and size control have a great impact in catalysis[4] and chirality.[9] For instance, many reported data in the absence of dedicated hole scavenger (MeOH, EtOH,…), gave deposition results which varied from each other,[20, 26-27, 30, 36, 38, 40-42] and where the true effect of parameters such as the Au/DRs ratio, and the role and ratio of hole scavenger were not specifically identified. The same statement can be made about the effects of light intensity when considering photodeposition. This is probably the reason why the actual results, reported so far, vary so much from one experiment to another (see Supporting Information **Table S1**).

We propose to fill in this gap in the present work. To do so, we choose laser photodeposition and use light intensity as an additional control compared to classical chemical reduction schemes. We build-up a specific set-up using a focused laser beam, to properly tune photon fluxes and get high electron-hole pairs production rates, and we investigate laser-induced gold nanodots (NDs) growth on DRs. We also proceed to a systematic study of the variation of the ratio between single, double, and multiple sites, which provides guidance for future research by playing with the following parameters. First of all, we use methanol (MeOH) as a hole scavenger and vary its concentration; doing so we show that it plays a key role for the single-tip deposition, and provides a mild reagent to

improve the *operability* and *reproducibility* of the experimental results. We then varied the concentration of the stable $KAuCl_4$ as a gold precursor, without any additional ligands injection at room temperature. Finally, as this gold ND size is of major importance for catalysis efficiency, modelling of the growth mechanisms also represents an issue to predict reproducibility. For the chemical reduction route, a pioneer lattice-gas modelling suggested gold growth at the two tips of the DRs followed by a late stage ripening process to shift from two-sided to single-tip growth.[24] Considering here photodeposition, we develop a specific model that now describes laser-induced gold NDs growth on DRs in varying chemical environment, and predicts the emergence of a single master behavior which compares well with experimental data, and shows that photodeposition is also a very efficient route to synthesize Au-CdSe/CdS NHDs with versatility and predictability. The generalization to other metal deposition is also illustrated using data from another pioneer work on laser-induced growth of platinum NDs onto CdS nanorods.[29]

RESULTS AND DISCUSSION

To better understand the significance of this work, and make a guide for straightforward understanding of the current progress in this field, we gathered other related works (Supporting Information **Table S1**) on the current metal deposition on cadmium chalcogenide semiconductors (Cadmium-based II–VI semiconductors), especially for in-depth analysis of the most studied gold deposition, which provides NHDs with a great potential for high performance catalysis. As shown in **Table S1**, different effects play a role: the reaction temperature, the ligands, the light-induced deposition, the reaction time, the type of semiconductors, and the type of gold precursors. The results comparisons are based on the deposition sites, such as Single-Tip (ST), Double-Tip (DT), and Multi-Sites (MS) distributions. The most effective methods now tend to lower the deposition temperature,[20, 26, 30, 36, 41-42] shorten the reaction time,[12, 20] and use long alkyl amine ligands;[20, 26, 41

laser or lamp-assisted photodeposition may also help in getting more selective ST deposition.[26, 29] In some few cases the hole scavenger was stated as such, and identified as a short chain alcohol (methanol, ethanol, isopropanol, ethylene glycol);[19, 43-46] but most of the time it is barely mentioned, and TEM images show quantum dots and DRs corrosion taking place concomitantly with the gold deposition.

Even if O'Sullivan *et al.* reported that the more active AuCl could achieve ST deposition in a much easier way than $AuCl_3$ and in a shorter time (< 120 s),[12] its uncontrollable "high reactivity" leads to simultaneous MS deposition of tiny Au NDs on the surface of the DRs. Moreover, it seems that most publications report *only* on the results of ST deposition with high probability, and there is still no literature on how to control accurately the deposition ratio of the different sites, *i.e.*, how to achieve true ST deposition in the statistical sense. Additionally, although Alivisatos' and Banin's groups successful initiated investigations based on the laser or lamp-induced photodeposition,[20, 26, 29, 38, 41] the effect of the light intensity still remains to be analyzed in details. Therefore, in this work, we focus on studying the variation in the ratio of photoproduced ST HNPs when using laser light to reach high electron-hole pairs production rates, with MeOH as dedicated hole scavenger and a low activity gold precursor ($KAuCl_4$).[40, 47] The goal is to establish well-defined conditions to provide reproducibility, improve the operability and repeatability of the experimental results regardless the varying conditions, and eventually offer predictability in HNPs synthesis.

Briefly, the DRs used along this work were prepared using 3.9 nm CdSe cores and grown at 350 ^{o}C. They have a diameter of 7.6 ± 0.8 nm (shell thickness of 1.84 nm) a length of 48.0 ± 2.1 nm leading to an aspect ratio (AR) of 6.3 (see **Figure S1** for their TEM images and spectroscopic data).

Setup and Methodology

Experiments were performed inside a square cuvette containing CdSe/CdS DRs covered with stabilizing ligands (ODPA/HPA), a dodecylamine (DDA) modified $KAuCl_4$ precursor in toluene[47] and MeOH as a hole scavenger. Due to the large volume of the CdS shell, its UV-vis absorption spectrum shows an excellent absorption in the blue range, which led us to choose the wavelength λ = 473 nm, within the bandgap of the DRs for laser-deposition experiments. A schematic drawing of the experimental setup is shown in **Figure S2**. After exiting from the laser head, the beam is set at the same height as the reaction cuvette using a periscope. Then two lenses, a cylindrical one (f = 200 mm) to correct the beam profile ellipticity, and a spherical one (f = 75 mm), are used to eventually set a round laser spot of 1 cm in diameter incident to the 1 cm wide cuvette. The cuvette (disposable 1×1×4 cm^3 filled with 1 cm^3 solution) is placed on a magnetic stirrer to continuously homogenize the DRs solution and prevent sedimentation; the stirring speed was set at 300 rpm. All experiments were performed at room temperature. The beam power range at the exit of the head varies from P_L = 0 to 390 mW when changing the driving current, with a maximum current of 5.0 A. With a transmission of the setup of P_i/P_L = 81%, the power range incident to the cuvette is P_i = 0 to 315 mW. Considering the transmission of the cuvette P_t/P_i = 74% when filled with a solution of concentration [DR] = 2.5 nM, the beam intensity I estimated in the middle of the cuvette is $I = 2(P_iP_t)^{1/2}/(\pi\omega^2)$ = 0 to 690 mW/cm^2 for a beam diameter 2ω = 1 cm. Finally, with steering and a transmission of 74%, we can assume that the 1 cm^3 solution is homogeneously exposed to light.

Control experiments

In order to study the influence of the different reaction parameters on the laser-deposition, we first performed some comparative ground experiments on DRs ([DR] = 2.5 nM) where the light excitation and the presence of MeOH were tested separately (**Figure S3**, **Table S2** and experimental section). On their own, both may trigger gold nucleation and growth, but the yield and the selectivity

are rather poor. Even if single-tip (ST) nanoheterodimers (NHDs) are produced in the absence of MeOH, the ratio of these ST NHDs is limited to about 40% and the combined ratio of DT + MS is as high the ST one. In the absence of photo-excitation, Au NDs could nucleate and grow on the DRs surface up to 2.3 nm after 8 min dark reaction with an overall ratio of 94% including 75 % MS. A comparison with Banin's group work, where 1.5-1.8 nm Au ND tip were obtained in the dark at room temperature after 1 hour,[20] suggests that without light exposure, MeOH can effectively increase the reaction rate and trigger nucleation at defects, with a prevailing MS (75%) deposition. In the absence of either of them, and still during a reaction time of 8 min (mainly used in the following for the laser deposition), the reactivity is low with gold NDs diameters $D < 2$ nm and a predominance of bare DRs (> 60 %).

We also studied the case when no DRs were added in the solution. Under laser excitation $I = 355$ mW/cm^2 and exposure times as long as 32 min, coupled with gold precursor concentrations as high as 160 µM, only very few small-size Au NDs, not even detectable by UV-vis spectroscopy, did form. This means that DDA modified $KAuCl_4$ in toluene in the presence of MeOH is stable enough for our photodeposition experiments to take place and will not affect the analysis of the experimental results (see **Figure S4** for the rare Au NDs found on the TEM grid).

In view of these experiments, we analyze in the following the influence of these different parameters involved in the photodeposition of gold NDs onto DRs, focusing on two major aspects: their influence on the distribution of the HNPs in between ST, DT and MS distributions, and the growth of the gold ND in the ST case.

Effect of hole scavenger on Au photodeposition

The light absorption within the bandgap of a semiconductor produces electron-hole pairs; using focused lasers, instead of lamps or LEDs, offers the opportunity to properly focus beams and get significant photons fluxes so that the electron-hole pair production can be controlled and

tremendously increased, and the charge availability is no more altered by their trapping on the semiconductor defects.[35] These electron-hole pairs may recombine but also reduce gold ions and concomitantly consume holes by some scavenging effect. In order to properly control this hole scavenging and since the reaction takes place in an organic phase, we chose methanol to play this role as it is fully miscible with toluene. Additionally, its scavenging efficiency in the presence of TiO_2 under UV excitation has been widely demonstrated,[35, 48] motivating us to explore its role in CdSe/CdS DRs systems. To check the scavenging effect of methanol, we chose to keep constant all the other parameters involved in the reaction: beam intensity inside the cuvette I = 355 mW/cm^2, [$KAuCl_4$] = 40 µM, [DR] = 2.5 nM, deposition time t = 8 min.

As shown in **Figure 1**, **Figure S5** and **Table S3**, the ratio of ST NHDs significantly increases just after adding the hole scavenger (from 42.1 % to 68.5%), and then grows up to at least 80% for [MeOH] ≥ 0.625 M. Concomitantly, as shown in **Figure 1e**, the DT and MS Au-DRs ratios decrease as [MeOH] increases, further confirming the key role of adding a dedicated hole scavenger for the laser-induced ST photodeposition as compared to the potential preexisting ones. The ratio of gold-free DRs remaining almost constant, MeOH and its concentration are definitely discriminant parameters since both DT and MS DRs significantly decrease to reach values around 2% (**Figure S5**), and [MeOH] = 1.2 M would be enough in these conditions. Going beyond this value, provides an increase of the ST gold ND size illustrated in **Figure 1f** (see also **Table S3**). This deposit size increased by 2 nm (from 3.8 to 5.8 nm **Table S3**) just after the addition of MeOH, which means that the hole scavenger not only controls the ratio of ST laser-deposition but also drives the gold ND growth at the tip of the DRs.[19]

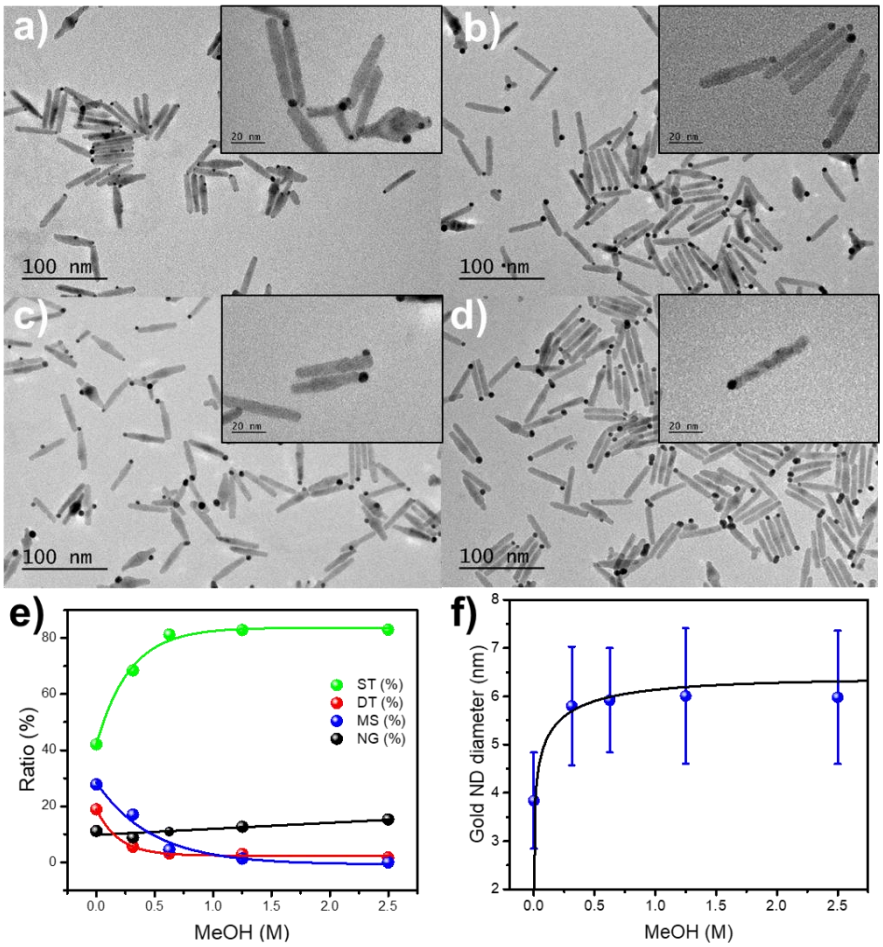

Figure 1. The effects of MeOH on the laser-deposition process. a) 0 M, b) 0.313 M, c) 0.625 M, d) 2.5 M; e) ratio variation of single-tip (ST), double-tip (DT), multi-sites (MS) HNPs and Au-free (NG) CdSe/CdS DRs (see also **Figure S5**); f) ST gold NDs growth *versus* methanol concentration; see modelling section for the fit explanation. [DR] = 2.5 nM, [Au^{3+}] = 40 µM, t = 8 min, beam intensity I = 355 mW/cm^2 (P_L = 200 mW).

As a final remark, since hole scavenging has been mention to participate to the surface etching of the DRs,[38-39] we also checked how the presence of methanol and its varying concentration could reduce this phenomenon. **Figure S6** shows its positive role on the integrity of the DRs length by reducing the damage from 5.6% (in the absence of MeOH) to 1.1%. This confirms that addition of MeOH significantly decreases the chalcogenide anions etching on the surface of DRs, thereby

reducing the number of defect sites for deposition and increasing the single-tip deposition ratio. It then appears that adding a hole scavenger on purpose, barely mentioned in photodeposition investigations on cadmium chalcogenide in the literature, is a real added-value for high yield ST deposition on CdSe/CdS DRs when its concentration is well-controlled, and may also explain why the results reported in the literature have been so scattered.

Effect of Laser beam intensity on Au photodeposition

Furthermore, the information about the light intensity applied to the mixture is often poorly described in the literature, while it is an essential parameter for the electron-hole pair production rate, as already demonstrated with the emergence of a high field regime, which promotes single dot deposition.[35] In these experiments, [MeOH] = 2.5 M, [DR] = 2.5 nM, [Au^{3+}] = 40 µM and deposition time t = 8 min. The representative TEM images of the Au-CdSe/CdS HNPs, obtained under beam intensities varying from I = 35 to 532 mW/cm^2 (P_L = 20, 50, 100, 300 mW) are illustrated in **Figure 2.** They have to be compared with the experiment performed in the dark where ST DRs are obtained with only 11.7% yield and gold NDs diameter of only 2.3 nm after 8 min (**Table S4 row 1** and **Figure S**7). The ratio of the ST deposition increases with the laser intensity (**Figure 2e**), and changes sharply from 11.7% to 67.4% just by using an exposure I = 35 mW/cm^2. This ratio still increases and maintains at a value higher than 80 % beyond I = 177 mW/cm^2 (P_L = 100 mW). This beam intensity threshold may be a signature of the crossover between the low and the high field growth regimes previously demonstrated in laser-deposition of silver and gold onto TiO_2 NPs as strongly beneficial for ST deposition.[35] This shows the importance of the laser irradiation for the ST deposition at a given hole scavenger concentration and the existence of a concentration threshold necessary to reach such high yields. Concomitantly, **Figure 2e** (see also **Figure S8**) shows that the presence of DT and MS Au-DRs decreases, raising the important role of light intensity, through the electron-hole production rate, in ST photodeposition. It also corroborates

the results obtained in photodeposition experiments using lamps (or LEDs) emitting typically a ten of mW/cm^2, known to produce MS deposition; this behavior is retrieved here at low laser intensity.[35]

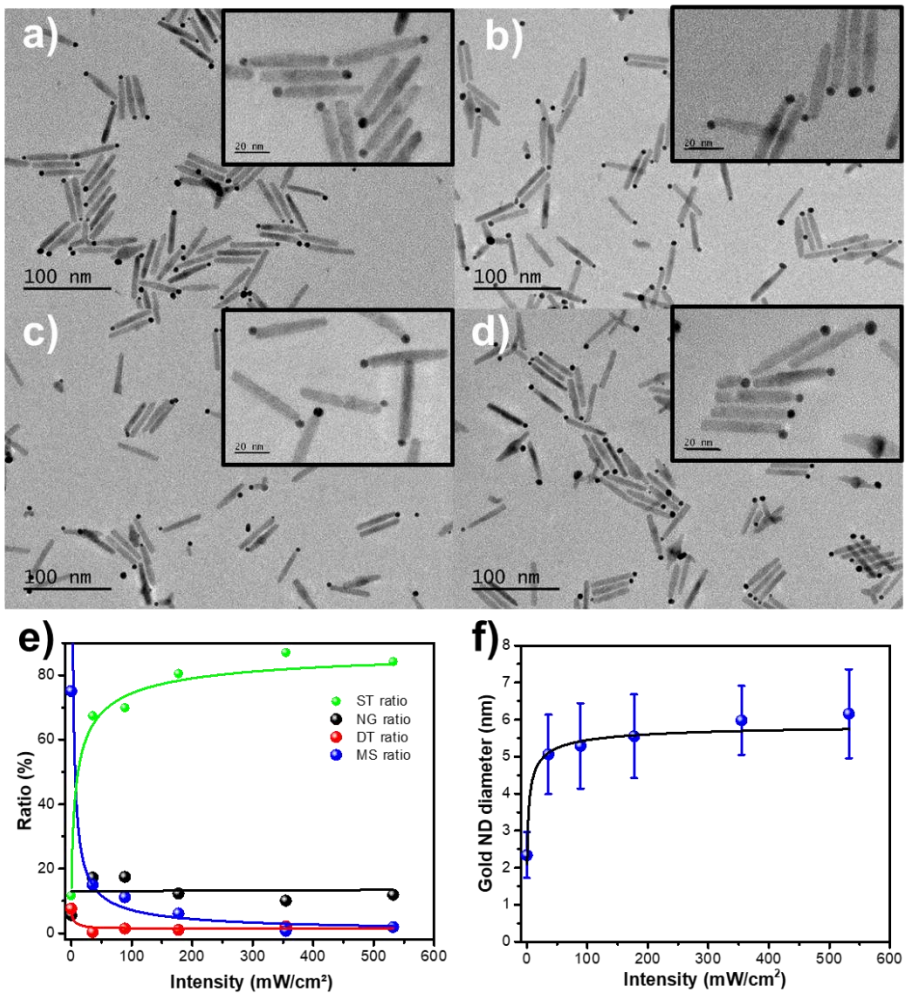

Figure 2. The effects of the beam intensity on the laser-deposition process. a) I = 35 mW/cm^2 (P_L = 20 mW), b) I = 89 mW/cm^2 (P_L = 50 mW), c) I = 177 mW/cm^2 (P_L = 100 mW), d) I = 532 mW/cm^2 (P_L = 300 mW); e) effects of the laser intensity on the gold nanodots distribution at the DRs surface with the ratio variation of ST, DT, MS HNPs and gold-free (NG) CdSe/CdS DRs (lines are guides for the eye); f) ST gold NDs growth *versus* beam intensity; see modelling section for the fit explanation. [MeOH] = 2.5 M, [DR] = 2.5 nM, [Au^{3+}] = 40 µM, t = 8 min.

Finally, **Figure 2f** provides the growth of the ST gold NDs with the beam intensity and shows that not only ST deposition is controlled by photon fluxes but also the size of the grown gold NDs. From now on, unless otherwise stated the ST and the sum of the contribution of DT and MS (DT + MS) will be shown on graphs as in **Figure S7** (see tables).

Effect of time exposure on Au photodeposition

The reaction time has been mentioned to play a significant role in controlling the deposition. However, there are also results at variance: (i) Pavlopoulos *et al.*[36] showed that MS were obtained at short times (< 30 s), and ripening took place to form ST NHDs for t > 2.5 min; (ii) O'Sullivan *et al.*[12] claimed that it was easy to achieve ST NHDs for t < 2 min; and (iii) Banin's group[20, 26, 41] found that ST NHDs were obtained under much longer deposition times (> 30 min) and at low temperature (< 277 K). These different results suggest that the underlying growth mechanism remains to be investigated.

Using laser-deposition, the ST, DT, MS and NG deposition distributions with and without a hole scavenger (**Figure S9**, **Tables S5** and **S6**) for three different exposure times show that as soon as MeOH is used as a hole scavenger (2.5 M), not only the ratio of ST NHDs is reached very fast (~ 4 min) and maintained at about 80% over time, but the MS deposition is reduced below 1%. Conversely, with no MeOH, the ST DRs ratio drops with time (from 44.9% to 25.4%) while the MS deposition sharply increases from 1.6% to 50.3%, explaining the diverse results published in the literature. This confirms again the crucial role played by the presence of a hole scavenger to obtain ST NHDs.

The effect of the laser irradiation time on the deposition, in the presence of MeOH and over long exposures up to 64 min (**Figure 3** and **Figure S10**), shows that the ratio of ST NHDs reaches values up to 87% for an optimum time of 8 min, and then slightly decreases for longer exposures even if

staying above 70%. This may be correlated with the variation of the DRs etching process since DRs are shortened by nearly 9 % at long irradiation times, despite the presence of MeOH as a hole scavenger (**Figures S11a** and **b**). Conversely, there is little change in the DRs length for short reaction times (< 8 min), and the etching ratio is maintained below 2 %.

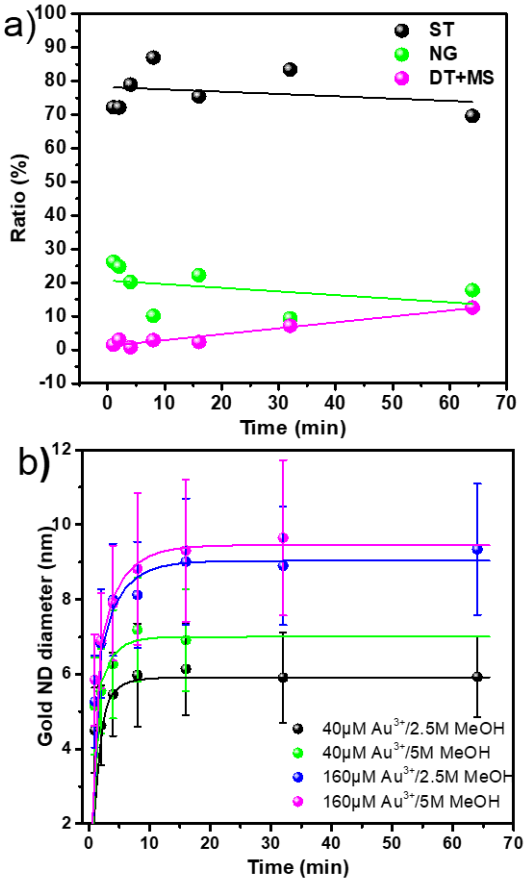

Figure 3. Dynamics of the laser-deposition with MeOH as a hole scavenger: a) Variation of the ST, DT+MS and NG deposition ratios for [MeOH] = 2.5 M, [Au^{3+}] = 40 μM. Lines are guides for the eye; b) ST Au NDs growth *versus* exposure time for different values of [MeOH] and [Au^{3+}] (see modelling section for the fit explanation). [MeOH] = 2.5 M, [Au^{3+}] = 40 μM, [DR] = 2.5 nM and I = 355 mW/cm^2 (P_L = 200 mW) for all experiments.

In the same way, in **Figure 3b**, the Au NDs diameter gradually increases with time, with a saturation phenomenon in between 16 and 32 min. Concomitant increase of the (DT + MS) DRs ratio and decrease of NG DRs ratio are observed.

Finally, the ST Au NDs growth illustrated in **Figure 3b** shows that the different dynamics seem self-similar when varying both [MeOH] and [Au^{3+}]; this self-similarity is investigated below with a growth modelling. Moreover, increasing [MeOH] by a factor of two at constant [Au^{3+}] has little influence on the final size of the Au NDs while increasing [Au^{3+}] by a factor of four at constant [MeOH] results in a fourfold increase of the final volume of the Au NDs. Consequently, if a hole scavenger is mandatory to achieve high yields of ST, the variation of [Au^{3+}] in the solution sensitively actuates the final size of the Au NDs and then provides control over the final HNDs produced. Some of the ST Au-modified DRs grown after 8 min were also analyzed by HAADF-STEM and energy dispersive X-ray (EDX); their elemental maps for S, Au, Cd, Se as well as EDX elemental mapping along a DR length (**Figure S12**) show the CdSe core in the medium of the DR, the CdS shell on each side along the whole length, the Au ND at the very tip of the rod. Note that some sulfur is also observed in the region of gold NDs which probably comes from the DR etching.

Gold concentration: effect of Au^{3+}/DRs ratio

We fixed the hole scavenger concentration ([MeOH] = 2.5 M), the laser intensity (I = 355 mW/cm^2) and the exposure time (t = 8 min). **Figure 4** and **Table S7** respectively show the TEM images, the distributions of the resulting Au-CdSe/CdS HNDs and the diameter variation of the ST gold NDs obtained at Au^{3+}/DRs ratios varying from 2000 to 128000. As [Au^{3+}] increases from 2.5 to 320 µM, the ST yield significantly increases from 2.1 % to 87 %, and then even up to 94 %. In view of the results presented in **Figure 4g,** we can infer that: (i) the ratio of ST NHDs increases with the

Au^{3+}/DRs ratio and then maintains at a high level (~ 90 %) as soon as [Au^{3+}] ≥ 40 µM; (ii) the NG ratio accordingly decreases; (iii) the (DT + MS) DRs are maintained constant at a low level.

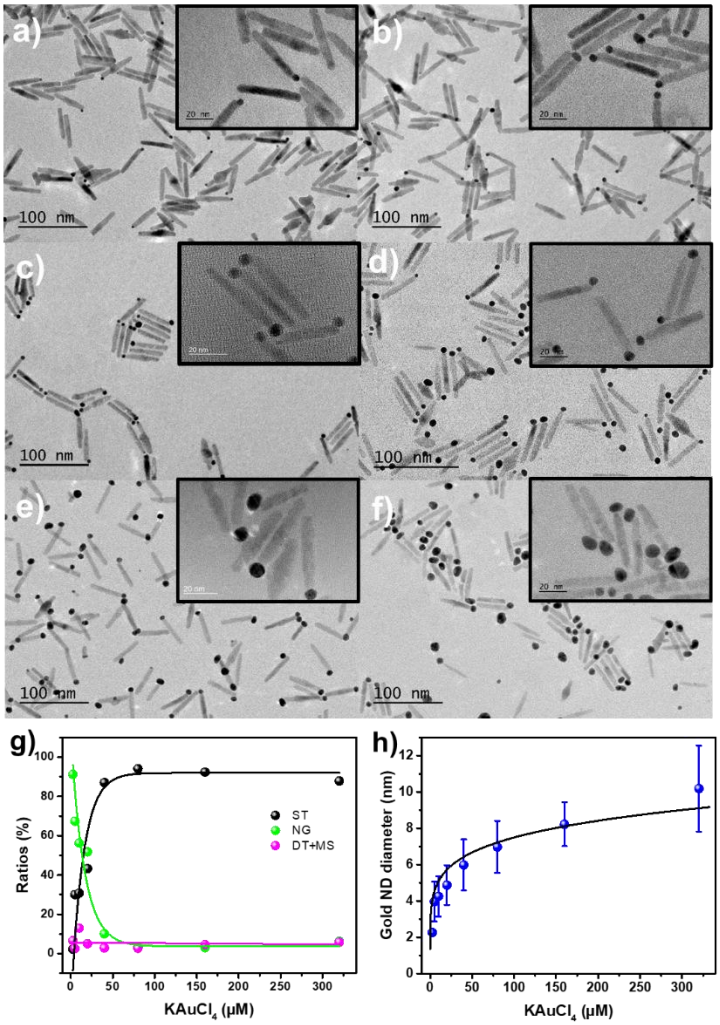

Figure 4. Effects of the Au^{3+}/DRs ratio on the photodeposition process when varying the concentration of the Au^{3+} precursor. a) 2000, b), 8000, c), 16000, d), 32000, e) 64000 f) 128000; g) Variation of ST NHDs, (DT + MS) HNPs, and NG CdSe/CdS DRs with gold-free deposition (lines are guides for the eyes). h) Variation of the Au ND diameter in ST NHDs (see modelling section for the fit explanation). [DR] = 2.5 nM, [MeOH] = 2.5 M, exposure time t = 8 min, I = 355 mW/cm^2 (P_L = 200 mW).

Moreover, **Figure 4h** shows that the gold diameter can be varied by a factor of 4-5 with the Au/DRs ratio (from 2.3 nm to 10.2 nm), and a high ratio of ST NHDs can be obtained from 6 nm to 10.2 nm at the used conditions. We also noted however that the DRs etching degree was Au^{3+} precursor concentration-dependent (**Figure S13**); it can be maintained to less than 2% as long as $[Au^{3+}] \leq 40$ µM and then gradually increases.

Finally, we varied the ratio of Au^{3+}/DRs by changing the concentration of CdSe/CdS DRs and keeping all the other parameters constant. Results are illustrated in **Figure 5** for [MeOH] = 2.5 M, $[Au^{3+}]$ = 40 µM, t = 8 min and I = 355 mW/cm^2 (P_L = 200 mW). **Figure 5a** shows that the ratio of ST NHDs decreases drastically when increasing [DR] and NG DRs increases in opposite direction; at the same time the ratio of (DT + MS) HNPs remains stable at a value below 5%. We suggest the following explanation. Increasing the DRs concentration, statistically reduces the bulk volume per DR and then the mean quantity of Au^{3+} available to grow a gold ND, so that nucleation conditions may become more and more sensitive to fluctuations in concentration. Since nucleation requires the crossing of an energy barrier on the one hand and growth is energetically more favorable than secondary nucleation on the other hand, the fact that the NRs are getting closer and closer by increasing their concentration will statistically favor in return the growth of already nucleated gold NDs. This could explain why the number of ST NHDs decreases after 8 min exposure; the weak level of (DT + MS) HNPs is also coherent with this statistical point of view.

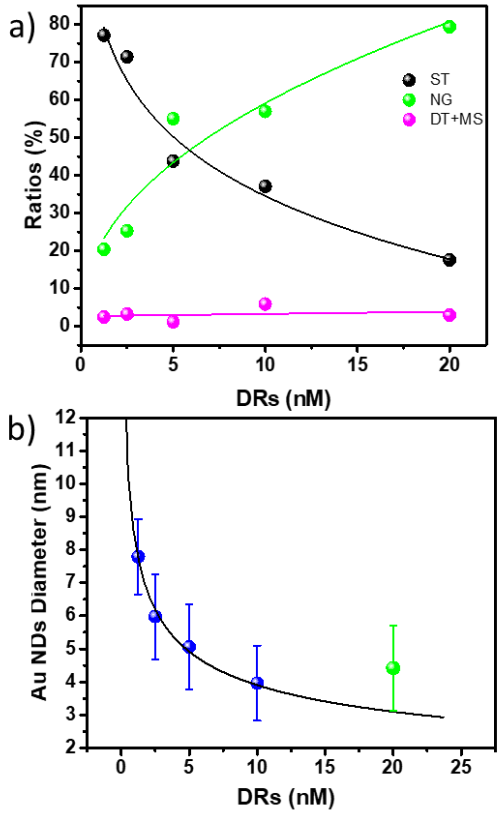

Figure 5. Variation of the concentration of CdSe/CdS DRs [DR] at constant [Au^{3+}]. a) Variation of ST NHDs, (DT + MS) HNPs, and gold-free (NG) CdSe/CdS DRs with the concentration of CdSe/CdS DRs (lines are guides for the eyes). b) Variation of the Au ND diameter of ST NHDs with DRs concentration (see modelling section for the fit explanation). [MeOH] = 2.5 M, [Au^{3+}] = 40 µM, exposure time t = 8 min, I = 355 mW/cm^2 (P_L = 200 mW). Note that the green dot is at the limit of coherence likely because only 17 % of ST NHDs are formed at [DR] = 20 nM.

Furthermore, looking at the growth of the ST NHDs (**Figure 5b**), it appears that the Au ND size decreases when increasing [DR]. This can easily be understood from mass conservation and statistical repartition arguments illustrated below by the growth modelling of the Au NDs on the DRs tip.

In the next section we will intend to developed a growth model of Au NDs onto CdSe/CdS DRs in order to quantitatively understand the previous behaviors measured as a function of the various parameters involved (beam intensity *I*, exposure time *t*, [MeOH], [Au^{3+}] and [DR]), and raise a master growth behavior that would account for all of them and predict laser-induced single ND deposition for general conditions.

Gold ND growth model and comparison to experiments

Testing all of these parameters, we collected experimental data that, in addition to the variation in the ratio of single-, dual-, and multi-site NHPs, seemed to reveal that the diameter of the grown gold NDs also depends on the concentrations of MeOH and Au^{3+}, the exposure time, and the laser intensity. We therefore try to interpret these data in the spirit of a built-in model previously used for the growth of metal NDs on TiO_2 nanoparticles when flowing solutions in open microchannels.[35] The goal, here, is to answer the two following questions: (i) Does a model developed for laser deposition in aqueous solution continue to make sense for describing ST ND growth onto CdSe/CdS DRs in organic solvents where metal ion adsorption conditions are radically different? (ii) Is this model, developed for ND growth in open channels where the metal ion concentration can be considered as constant, extendable to the finite volume case where metal ions are significantly consumed and growth completion is expected?

Assuming photoreduction of gold ions at the surface of the DRs, the total flux $\Phi(t)$ of gold atoms at the perimeter of the ND is proportional to the photoproduction rate of gold atoms $d[Au^0]/dt$; we find $\Phi(t) = (v_{Au}/[DR])\, d[Au^0]/dt$, where v_{Au} is the volume of a gold atom. As mass conservation imposes $\Phi(t) = (\kappa/8)D^2(dD/dt)$, where $\kappa(\theta) = (2/3 - cos\theta + cos^3\theta/3)$ is a dimensionless factor related to the contact angle θ of the gold ND at the tip of the DR,[49] we finally get the ND growth law (eq 1):

$$D^3(t) - D_c^3 = \frac{8}{\pi\kappa}\frac{\nu_{Au}}{[DR]}[Au^0](t), \quad (1)$$

where $t = 0$ s corresponds to the time when the laser exposure is switched on, $[Au^0](t = 0) = 0$, and $D(t = 0) = D_c$ is the nucleation diameter that will be neglected in the following since experiments are performed over long exposure times.

To calculate $[Au^0](t)$, we consider that the DRs are photo-excited in their bandgap according to the eq 2. Upon light absorption, electron-hole pairs are produced in the volume and at the surface of the DRs at a rate $g \propto \alpha I$ where α is the optical absorption of the solution at the used wavelength. The electrons, of concentration [e], either recombine with the holes with a rate k_r, are trapped on defects (we neglect this effect owing to the large amount of carriers produced from focused laser excitation), or reduce the Au^{3+} ions adsorbed at the surface of the DRs at an effective rate k_e. In an analogous way, holes, of concentration [h], either recombine with electrons, are trapped on defects (neglected for the same reason as electron trapping) or oxidize the hole scavenger HS (MeOH in the experiments) adsorbed at the surface of the DRs at a rate k_h. This scheme is summarized in eq 2:

$$\begin{cases} \left[\mathrm{DR} + h\nu(> E_{bg}) \underset{k_r}{\overset{g}{\rightleftharpoons}} \mathrm{DR}(e^-, h^+)\right]_{\text{bulk}}, \\ \left[\mathrm{HS} + h^+ \overset{k_h}{\rightarrow} \mathrm{HS}^+\right]_{\text{interface}}, \\ \left[\mathrm{Au}^{3+} + 3e^- \overset{k_e}{\rightarrow} \mathrm{Au}^0\right]_{\text{interface}}. \end{cases} \quad (2)$$

Since the carrier diffusion time inside the DRs is typically in the picosecond range, we assume that electrons and holes are rapidly distributed inside the DRs at time scales involved in gold ND growth so that the diffusion can be neglected and we can solve the following set of equations (eq 3):

$$\begin{cases} \dfrac{d[\mathrm{e}]}{dt} = \{g - k_r[\mathrm{e}]\cdot[\mathrm{h}]\}_{\text{bulk}} - \{k_e[\mathrm{e}]\cdot[\mathrm{Au}^{3+}]\}_{\text{ads}}, \quad (3a) \\ d[\mathrm{h}] \end{cases}$$

(3b)

(3c)

(3d)

Note that the diffusion of Au^0 atoms at DRs surface has also been neglected in eq 3d because a calculation shows that it is very small compared to the reaction term $\{k_e[\mathrm{e}] \cdot [Au^{3+}]\}_{\mathrm{ads}}$. Moreover, the hole scavenger being always in large excess in our experiments, we can consider [HS] as a constant in eq 3c all along the photoreaction. Finally, since we investigated ND growth over long time exposures, we can assume that the number of electron-hole pairs is equilibrated during the entire laser-deposition process so that $d[\mathrm{e}]/dt = d[\mathrm{h}]/dt$. Using this last property, eqs 3a-b allow to determine the dynamics of the electron concentration (eq 4):

$$\frac{d[\mathrm{e}]}{dt} = g - k_e[\mathrm{e}] \cdot [Au^{3+}]_{ads}\left(\frac{k_r}{k_h[\mathrm{HS}]_{ads}}[\mathrm{e}] + 1\right) \quad (4)$$

This equation, coupled to $d[Au^0]/dt = -d[Au^{3+}]_{ads}/dt = \{k_e[\mathrm{e}] \cdot [Au^{3+}]\}_{\mathrm{ads}}$ (eq 3d), cannot be solved analytically when $[Au^{3+}]$ is temporally consumed during the photoreaction to produced $[Au^0]$. So, looking at the late stage growth of the gold NDs triggered by focused lasers we propose an already established simpler route[35] which showed that the electron concentration in high field conditions ($k_r[\mathrm{e}]/(k_h[\mathrm{HS}]) \gg 1$, fulfilled when using focused laser excitations) is already stationary: $[e](t) \approx [\mathrm{e}]_{sta} = \sqrt{k_h[\mathrm{HS}]g/(k_r k_e[Au^{3+}]_{ads})}$. Then, the solution of eq 3d is (eq 5):

$$[Au^0](t) \approx [Au^{3+}]_{ads}^{max} \cdot \frac{t}{\tau}\left|1 - \frac{t}{4\tau}\right|. \quad (5)$$

$\tau = \sqrt{k_r[Au^{3+}]_{ads}^{max}/(k_e k_h[\mathrm{HS}]_{ads} \cdot g)}$ is the characteristic reaction time scale, where $[Au^{3+}]_{ads}^{max}$ represents the largest concentration that can be adsorbed up to completion of the laser-deposition in a finite volume solution. However, since completion of the reaction is expected at long exposure time, the behavior given by eq 5 may eventually become unphysical because the increase of $[\mathrm{e}]_{\mathrm{sta}}$,

due to $[Au^{3+}]_{ads}$ consumption, cannot diverge in a finite size DR and should eventually saturate to the value $[e]_{sat} = \sqrt{g/k_r}$, given by the balance between the production of electrons and their recombination. Then, there is a time t^* for the photoreaction dynamics such that $[e]_{sta}(t^*) \sim [e]_{sat}$, and eq. 3d shows that $[Au^0](t > t^*)$ should saturate exponentially. Consequently, the late stage growth of the volume of a gold ND at the tip of a DR is predicted to be linear in time ($t/\tau < 4$, eq 5), followed by a parabolic crossover (eq 5) to an exponential saturation at long times; note that the linear behavior corresponds exactly to the growth prediction obtained at constant gold ion concentration when flowing the solution in a microchannel.[35] Finally, by injecting the calculated gold concentration $[Au^0](t)$ into the predicted growth law for NDs (eq 1), our modelling suggests that our set of ST ND growth data, obtained by varying the different involved parameters and concentrations, should collapse onto a single master behavior when rescaling time *t* by τ (deduced from the variations of $[Au^0]$, eq 5) and the gold ND volume by $[Au^{3+}]_{ads}^{max}/[DR]$ (deduced from mass conservation, eq 1). To check this scaling, we first need to discuss the different terms involved.

Since in toluene the DRs are covered of stabilizing ligands (ODPA/HPA) and gold ions $AuCl_4^-$ are solubilized using DDA, the concentrations $[Au^{3+}]_{ads}$ and $[HS]_{ads}$, which react with the electrons and holes produced by laser absorption, cannot be related to their bulk values $[Au^{3+}]$ and [HS] by a Langmuir isotherm, as classically expected for free $AuCl_4^-$ on the ligand-free surface of metal oxide NPs in aqueous solutions.[50] While the small size of MeOH may help penetration of the protective layer of ODPA/HPA along the length at the DRs and then adsorption at their surface, this is not possible for the solubilized gold ions which then take advantage of the tip morphology and the less dense disposition of the ligands for their own approach of the DRs. So the presence of stabilizing ligands on DRs and large solubilizing agents for gold does not favor any specific adsorption and we can simply assume that $[Au^{3+}]_{ads} \propto [Au^{3+}]$ and $[HS]_{ads} \propto [HS]$, as suggested by Mills *et al.*[51]

Moreover, the rate of electron-hole pairs produced by the laser excitation is given by $g = \alpha I/(10^3 N_A \hbar\omega)$ M/s,[35] where N_A is the Avogadro's number and $\hbar\omega$ the energy of the used photons. Using the definition $\alpha = \sigma_{abs} \cdot (N/V)$, where *N/V* is the number of DRs per unit volume and σ_{abs} their absorption cross-section (which can be estimated in the Rayleigh regime when considering DRs as ellipsoidal), we simply deduce $\alpha \propto [\mathrm{DR}]$ so that $g \propto I \cdot [\mathrm{DR}]$. Finally, in the absence of a complete data set for the reaction rates k_r, k_e and k_h involved in the definition of the time scale τ, we will consider them as constant during the laser-deposition process. Then, noting $[\mathrm{Au}^{3+}]_0 = [\mathrm{Au}^{3+}](t = 0)$ and writing $[\mathrm{Au}^{3+}]_{ads}^{max} = \beta[\mathrm{Au}^{3+}]_0$ where β is the ratio of gold ions consumed at completion, eq 1 predicts a gold ND growth law $D^3(t/\tau) \approx \frac{8}{\pi\kappa}\frac{v_{Au}}{[DR]}[\mathrm{Au}^0](t/\tau) = \frac{8v_{Au}}{\pi\kappa}\beta\frac{[\mathrm{Au}^{3+}]_0}{[\mathrm{DR}]}f(t/\tau)$, where $f(t/\tau)$ is given by eq 5 at the early stage followed by an exponential saturation satisfying $f(t/\tau \to \infty) = 1$. We check this master behavior by plotting in **Figure 6**, $D \cdot ([\mathrm{DR}]/[\mathrm{Au}^{3+}]_0)^{1/3}$ as a function of $t/\tau \propto \sqrt{[\mathrm{MeOH}] \cdot [\mathrm{DR}] \cdot I/[\mathrm{Au}^{3+}]_0} \cdot t$ for the whole data set presented in **Figure 1**-**Figure 5** for the ST gold ND growth as a function of the different involved parameters.

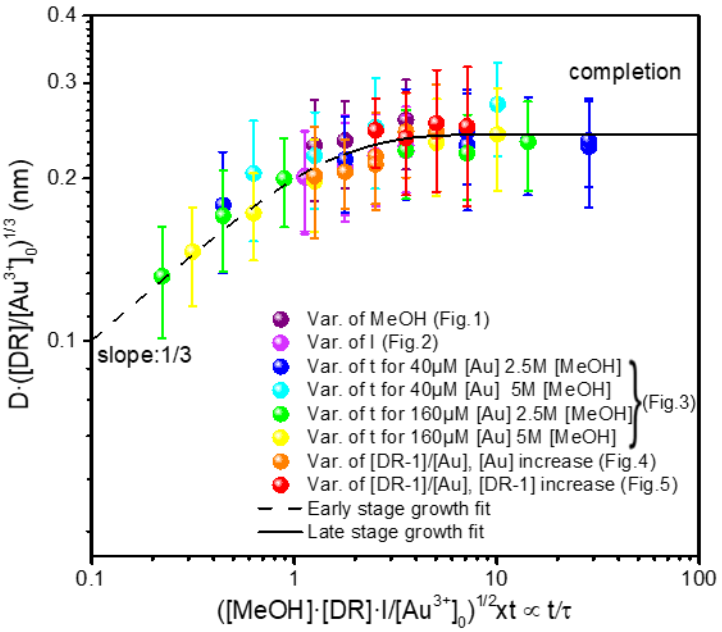

Figure 6. Plot of the rescaled single tip gold ND diameter $D \cdot ([\mathrm{DR}]/[\mathrm{Au}^{3+}]_0)^{1/3}$ as a function of the rescaled time $t/\tau \propto \sqrt{[\mathrm{MeOH}] \cdot [\mathrm{DR}] \cdot I/[\mathrm{Au}^{3+}]_0} \cdot t$ when varying the methanol concentration [HS] (**Figure 1**), the beam intensity I (**Figure 2**), the exposure time t at two gold ion and two methanol concentrations (**Figure 3**), the initial gold ion concentration $[\mathrm{Au}^{3+}]_0$ (**Figure 4**) and the concentration in DRs (**Figure 5**), all other parameters being fixed for each experiment. The fitting curve is composed of two successive behaviors, the early one predicted by eq 5 and starting with an exponent 1/3 associated to $[\mathrm{Au}^{3+}](t) \approx [\mathrm{Au}^{3+}]_0$ at early stage, followed by an exponential saturation in t/τ up to completion of the photoreaction in the finite volume solution (1 cm^3). The error on the ND diameter corresponds to the standard deviation obtained from at least 200-250 measurements.

Figure 6 indeed confirms that experiments performed for varying exposure times, beam intensities, hole scavenger and gold ion concentrations, and DR concentrations, indicated by different colors, all rescale onto a single 'master curve' over more than two orders of magnitude of

rescaled time t/τ. The behavior $D\sim(t/\tau)^{1/3}$, expected for the ND growth at early stage when driven by an almost constant flux of gold atoms and already demonstrated for metal ND growth on metal oxide NPs in aqueous solutions,[35] is retrieved here at the beginning of the investigated range of rescaled time when $[\mathrm{Au}^{3+}](t) \approx [\mathrm{Au}^{3+}]_0$. The rescaling continues with the slowing down of the dynamics due to gold ion consumption and ends up with the expected saturation that indicates the growth completion at late time; a two-behavior fit according to the model gives a correlation close to 0.9. By performing experiments with varying $[\mathrm{Au}^{3+}]_0$ and [DR], **Figure 6** shows as well that the expected behavior for the final ND diameter $D_\infty = \left(\frac{8\nu_{Au}}{\pi\kappa}\beta\right)^{1/3} \cdot ([\mathrm{Au}^{3+}]_0/[\mathrm{DR}])^{1/3}$ is experimentally retrieved for ST NHDs. Moreover, even if the hole scavenging is a corner stone for the ST NHDs production, D_∞ is independent of [MeOH] for the investigated range (0.5-5 M) as already observed experimentally (**Figure 3**) and theoretically expected when charge transfers are equilibrated. Finally, one can use the expression of D_∞, to estimate the amount of gold deposited at completion $[Au^0]/[Au^{3+}]_0$ from mass conservation (at completion, $[Au^0] = [\mathrm{Au}^{3+}]_{ads}^{max}$). If Y_{exp} denotes the measured yield for ST deposition, the ratio of deposited gold at completion is given by (eq 6):

$$\frac{[\mathrm{Au}^0]}{[\mathrm{Au}^{3+}]_0} \equiv \frac{[\mathrm{Au}^{3+}]_{ads}^{max}}{[\mathrm{Au}^{3+}]_0} = \beta = \frac{Y_{exp}}{\nu_{Au}} \frac{[\mathrm{DR}]}{[\mathrm{Au}^{3+}]_0} \frac{\pi\kappa(\theta)}{8} {D_\infty}^3. \quad (6)$$

We deduce $([\mathrm{DR}]/[\mathrm{Au}^{3+}]_0){D_\infty}^3 = 0.24^3$ nm^3 from the fit of the data rescaling shown in **Figure 6** and experimental results give a mean yield $Y_{exp} \geq 80\%$ (**Figure 1**-**Figure 5**). Considering as well the large contact angle observed experimentally (**Figure 3d**), $\kappa \approx 4/3$, and using $\nu_{Au} = M_{Au}/(N_A \varrho_{Au})$, where $M_{Au} = 196.97$ g and $\rho_{Au} = 19.3\ \mathrm{g}/cm^3$ are the gold molar mass and density, we finally find $\beta = [Au^0]/[Au^{3+}]_0 \geq 34\%$. This ratio shows that only one third of the initial gold ion concentration has been photoreduced at completion and suggests that the gold ND growth is

eventually limited geometrically by the presence of stabilizing ligands at the DR surface developed parallel to its (001) axis. This mainly constrain the Au^{3+} adsorption onto the tip, and the ND growth continuously reduces this adsorption surface area so that the number of available photoproduced gold atoms decreases until it becomes almost negligible. As a consequence, the gold ND growth saturates. This completion before total consumption nicely correlates with the detachment of gold ND from the tip when its size reaches or exceeds the DR diameter, as previously discussed (**Figure 3c)**.

So the ST growth on CdSe/CdS DRs can be quantitatively understood from the constant concentration regime ($D \sim (t/\tau)^{1/3}$) up to completion ($D \sim (t/\tau)^{0}$). Moreoever, when the final size of the reaction product matters more than dynamics, D_∞ can not only be predicted but also easily tuned by varying $[Au^{3+}]_0$ or [DR] to reach targeted sizes for dedicated applications.

Chemical nature of the hole scavenger

The last aspect to check was the influence of the chemical nature of the hole scavenger. We then compared three alcohols with increasing chain length at the same volume fraction of 10 % v/v: methanol (2.5 M), ethanol (1.7 M) and isopropanol (1.3 M).

Figure 7 shows that here too the choice of the reagent is not trivial. The chain length as well as the steric hindrance decrease the gold ND size, all the other parameters being identical, and suggest methanol as the best choice.

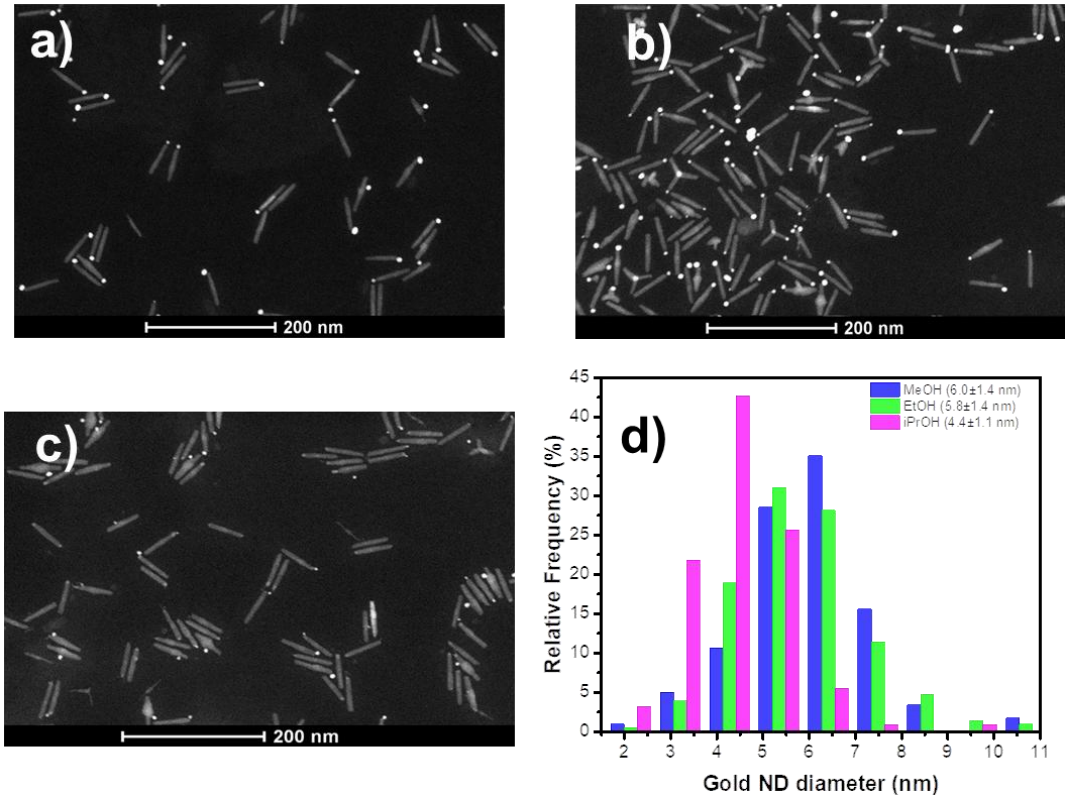

Figure 7. Effects of the chemical nature of the hole scavenger (10% v/v) on the gold NDs size: high-angle annular dark-field scanning transmission electron microscopy (HAADF-STEM) images of Au ST NHDs with a) MeOH b) EtOH and c) iPrOH as hole scavengers; d) size distribution obtained with methanol (2.5 M), ethanol (1.7 M) and isopropanol (1.3 M) as hole scavengers. [DR] = 2.5 nM, $[Au^{3+}]$ = 40 µM, time t = 8 min, I = 355 mW/cm^2 (P_L = 200 mW).

Confrontation to literature data

Finally, despite the importance of metal loaded II-VI semiconductors NPs in photocatalysis, we are aware of very few publications where the metallic ND growth by photodeposition has been investigated in detail. In a pioneer investigation, Dukovic *et al.*[29] analyzed the growth of platinum NDs onto CdS NRs in the presence of an excess of tertiary amine (triethylamine and diisopropylethylamine) in toluene using photoexcitation by a continuous Ar^+ laser working at λ = 458 nm. On the one hand, they analyzed the ratio between single-, double- and multi-deposition, and

Pt-free NRs as a function of the exposure time. On the other hand, they investigated the effects of the exposure time *t*, beam power *P*, initial concentration $[Pt^{2+}]_0$ of platinum precursor ((1,5-cyclooctadiene)dimethylplatinum(II)) and concentration of CdS units; the effect of CdS unit variation will not be discussed in the following due to the small range of the data set. Experiments were performed in borosilicate NMR tubes so that 50 % of the beam section was effectively used for laser-deposition and, after showing morphologies of the induced NHRs by TEM images, the ND growth onto CdS NRs was analyzed by ICP to get the atomic mass ratio Pt/Cd; standard conditions for the non-varying variables were: t = 60 min, P = 100 mW, $[Pt^{2+}]_0 = 10$ mM, and $[CdS] = 10$ mM. They first found that the nucleation process of platinum NDs did not evolve with time so that the yields in single-, double-, multi-deposition, and platinum -free NRs remained constant during the growth; the mean deposition yield Y_{exp} can thus be assumed as constant at first sight. Then, they showed that the mass ratio Pt/Cd behaved linearly in time exposure (**Figure 8 insert a**), and increased nonlinearly with the exciting beam power *P* (**Figure 8 insert b)** and the concentration $[Pt^{2+}]_0$ (**Figure 8 insert c**).

Using mass relations, the ratio Pt/Cd can be related to the different involved variables in the following way: $Pt/Cd \propto Y_{exp}\, D^3/[DR]$ with Y_{exp} constant, $D^3(t) \propto [Pt^0](t)/[DR]$ (as in eq. 1 for gold) and $[Pt^0](t) = [Pt^{2+}]_{ads}^{max} \cdot f(t/\tau)$, where the function $f(t/\tau)$ exhibits a linear behavior in rescaled time followed by a parabolic behavior (as in eq. 5) and a final exponential saturation satisfying $f(t/\tau \to \infty) = 1$, with $t/\tau \propto \sqrt{[HS]_{ads} \cdot [DR] \cdot P/[Pt^{2+}]_{ads}^{max}} \cdot t$. Then, writing $[Pt^{2+}]_{ads}^{max} = \beta[Pt^{2+}]_0$ on the one hand and considering on the other hand the measured linear variation in time exposure of the mass ratio Pt/Cd (**Figure 8a**, $t/\tau < 4$, eq 5) which strongly suggests that growth is far from completion, we expect $[Pt^0](t) \approx \beta[Pt^{2+}]_0 \cdot t/\tau$ and finally

$\mathrm{Pt/Cd} \propto D^3(t/\tau < 4) \propto \sqrt{[\mathrm{Pt}^{2+}]_0 \cdot P} \cdot t$ at constant [HS] (as in Dukovic *et al.*[29]) and [DR] (not considering the three measurements presented).

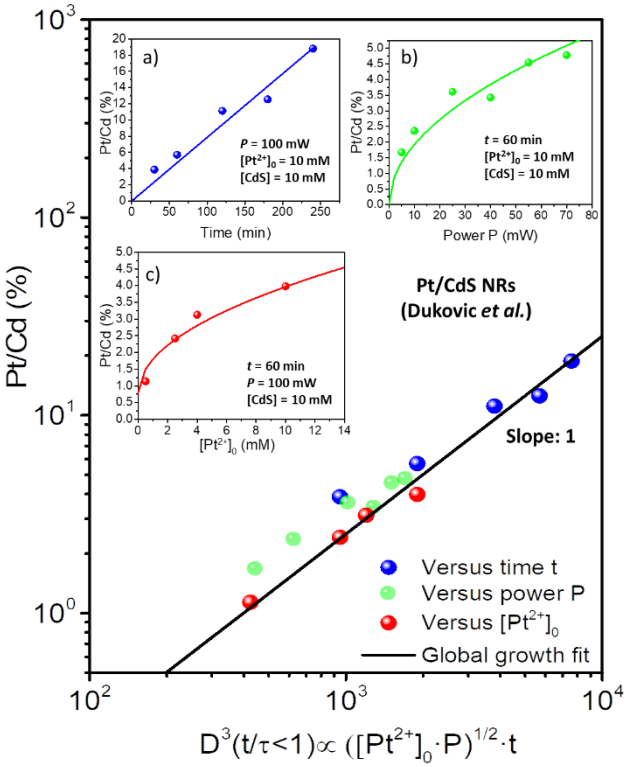

Figure 8. Master behavior of the Pt/Cd % variation when rescaled according to laser-driven ND growth onto NRs. Insets 8a-c) Pt/Cd % variation, induced by the platinum ND growth at the surface of CdS NRs, investigated by Dukovic *et al.*[29] as a function of the exposure time t (a), of the exciting beam power P (b) and of the initial concentration $[\mathrm{Pt}^{2+}]_0$ of platinum precursor (c); modelling suggests $\mathrm{Pt/Cd} \propto t$ (a), $\mathrm{Pt/Cd} \propto \sqrt{P}$ (b) and $\mathrm{Pt/Cd} \propto \sqrt{[\mathrm{Pt}^{2+}]_0}$ (c) illustrated by the different fits. When not varying, the values of the other quantities are: t = 60 min, P = 100 mW, $[\mathrm{Pt}^{2+}]_0 =$ 10 mM, and $[\mathrm{CdS}] = 10$ mM.

As shown in **Figure 8**, the proposed scaling to interpret the ICP measurements allows indeed the emergence of a single master behavior expected from the collapse of the different data variations with time, power and platinum ion concentration. Moreover, while the correlation of a linear fit is

better than 0.96, a pure power law fit of the data plotted in log-log scales in **Figure 8** gives a free exponent of 0.9, instead of 1, with just one order of magnitude in rescaled time, so that the expected linearity is quite well established. Consequently, Dukovic's investigation of Pt NDs growth onto CdS NRs can be interpreted within the frame of our modelling in terms of scaling. These findings were further confirmed by other experiments. For instance, analyzing gold deposition on CdSe/CdS DRs under ordinary UV lamp exposure, Carbone *et al.*[19] showed that the NDs volume linearly increased with time, as in the case of Dukovic *et al.*,[29] and as expected from the model in its early time interval ($t/\tau < 4$) of the late-stage growth at high field. Using analog protocols, Dermotière *et al.*[25] also investigated the gold deposition at the tip of CdSe/CdS DRs using a UV lamp and showed again with great precision that the average diameter of the gold NDs behaved as $D \sim t^{1/3}$, in excellent compatibility with previous experiments and actual modelling.

CONCLUSION

Considering the importance of metal loaded II-VI semiconductors NPs, and the difficulties to obtain ST deposition in a versatile way, we chose a laser-based photodeposition approach to revisit the nucleation and growth of gold NDs onto CdSe/CdS DRs in toluene as a model system. While focused lasers are essential to achieve high rates of electron-hole pair production, we have demonstrated that dedicated hole scavenging also plays a key role for the reliable production of ST NHPs. Through a comprehensive analysis of a combination of hole scavenger concentration, light intensity, deposition time and Au/DRs ratio, we have shown that all these factors play at their level a vital role in both the ST deposition process and in controlling the size of the deposited ND. 1) The addition of a tiny hole scavenger ([MeOH] > 0.625 M) when the solution is significantly irradiated (I > 177 mW/cm^2) is compulsory to decrease the double and multi-sites deposition, with almost

negligible contribution from gold-free DRs. 2) The Au^{3+}/DRs ratio is a key factor in decreasing the ratio of gold-free DR (with little contribution of double & multi-sites deposition), keeping the ratio of ST NHDs high, and tuning the final size of NDs on ST NHPs after completion. 3) The reaction time plays a minor role in the initial ST deposition (too long exposures favor DRs etching and a gradual increase of (DT+MS) deposition), but it also controls the size of NDs. 4) The modelling brings together the whole set of experiments on a single master curve showing how the ST gold ND growth collectively depends on the hole scavenger and gold precursor concentrations (chemical parameters) as well as exposure time and light intensity (physical parameters). 5) This master behavior allows not only to describe ST ND growth to completion but also to predict its final size and how to reach it for varying experimental conditions in organic solvent. 6) Finally we successfully interpreted experimental data extracted from the literature on platinum ND growth onto CdS NRs within the frame of our modelling in terms of collective scaling behavior. In conclusion, the production of ST metal loaded II-VI NPs by photodeposition in organic solvent can be made reliable and versatile, controllable and highly predictable provided electron-hole pairs are produced at a high rate and dedicated hole scavengers are significantly present.

Experimental Section

Chemicals: Tri-*n*-octylphosphine oxide (TOPO, 99%), tri-n-octylphosphine (TOP, 97%), tributylphosphine (TBP, 99%), *n*-octadecylphosphonic acid (ODPA, 97%) and *n*-hexylphosphonic acid (HPA, 97%) were purchased from Strem Chemicals. Cadmium oxide (CdO, 99.99%), sulfur (S, 99.98%), selenium (Se, 99.99%), potassium gold (III) chloride ($KAuCl_4$, 99.995%), dodecylamine (DDA, 98%), chloroform ($CHCl_3$, 99.0-99.4%, ~ 1% ethanol as stabilizer), and toluene (99.8%) were purchased from Sigma-Aldrich. All chemicals were used as received without further purification.

Materials: A MLL-N-473nm-300mW-19012905 (PO#G1900567) blue laser from the CNI company was used for the photochemical deposition. The TEM grid preparation is performed according to the following procedures: The solution is sonicated for 10 min to disperse the nanoparticles, and then one drop (~3-5 μL) is deposited on a TEM grid. A paper tissue can help absorb the liquid from the carbon film side from the back side of the grid, which allows only the liquid to pass through, and leaves the nanoparticles on the top side. Two or more $CHCl_3$ drops are also deposited onside, to wash away the remaining unreacted metal salts if any on DRs. Transmission electron microscopy (TEM) experiments were carried out with three machines, a JEOL JEM1400 Plus microscope operating at 120 kV, a Tecnai G2 F20 S-TWIN microscope operating at 200 kV, and a FEI Tecnai G2 F30 operating at 300 kV. High-resolution (HR) TEM images were obtained with a FEI Tecnai G2 F30 at 300 kV. The high-angle annular dark-field scanning transmission electron microscopy (HAADF-STEM) and energy dispersive X-ray (EDX) spectra were performed using a FEI Talos F200S microscope with an accelerating voltage of 200 kV. Moreover, in order to be representative and statistically meaningful, many images from several regions of various samples were recorded and the most characteristic results are presented here, and at least 200-250 NPs were treated. The UV-vis absorption spectra were recorded with 3600 Shimadzu UV-Vis-NIR spectrophotometer using 1cm quartz cuvettes. The PL spectra were recorded on a fluoroSENS spectrophotometer (Gilden Photonics).

Synthesis of spherical CdSe seeds

The synthetic procedure was based on the procedure reported in the literature.[52-54] Typically, TOPO (1.5 g), ODPA (0.140 g) and CdO (0.030 g) were mixed in a 50 mL flask, heated to 150 °C and alternately exposed to vacuum and argon at least 5 times until CdO was a brown solid and the rest of the reagents were a colorless liquid. Then, to dissolve the CdO, the solution was heated to above 320 °C under argon until it became optically clear and colorless, which indicated that the

reaction between CdO and ODPA was complete. Then, the temperature was increased to 350 °C, and 1.5 mL of TOP was injected into the flask, which caused the temperature to naturally decrease to 300 °C. Then, a Se:TOP solution (0.4 mL, 1 mol/L) was injected at 380 °C and reacted for several seconds. The size of the CdSe core was adjusted by controlling the temperature and reaction time.

The reaction mixture was cooled to 70~80 °C, and 8 mL of ethanol and 0.2 ml of TBP was added into the above solution, which was centrifuged at 10,000 rpm for 3 minutes. Then, the precipitate was dissolved in 2 ml of toluene while the supernatant was discarded. After centrifugation again, the precipitate was dissolved in TOP (CdSe-TOP).

Synthesis of CdSe/CdS DRs

In a typical synthesis of CdSe/CdS DRs *via* seeded growth, CdO (30 mg) was mixed in a 50 mL flask together with TOPO (1 g), ODPA (100 mg) and HPA (30 mg). After alternately exposing the flask to *vacuum* and argon at least 5 times at 150 °C for more than 1 h, the resulting solution was heated to 300 °C to make the solution become completely transparent liquid without any solid. Then, the temperature was increased to 350 °C and a mixed solution of S:TOP (0.5 mL, 2.5 mol/L) and the above CdSe-TOP solution (100 μL) was injected into the flask, which caused the temperature to naturally decrease to ~310 °C, and then recover to the pre-injection temperature within two minutes. The CdSe/CdS DRs were allowed to grow for 8 minutes after the injection. Finally, the reaction mixture was cooled to room temperature, and an extraction procedure was used to separate the nanocrystals from the side products and unreacted precursors.

General procedure for phase transfer of Au^{3+} precursor in toluene

For the preparation of the Au^{3+} precursor, 10 mM $KAuCl_4$ (0.1 mmol, 37.8 mg) were dissolved in water (10 mL), yielding a homogenous clear solution. This will subsequently be referred to as the Au^{3+} solution and diluted for phase transfer. The transfer of $KAuCl_4$ from water to toluene was performed following a procedure by Yang *et al.*[47] All the solutions before mixing were degassed by

bubbling argon for 10 min. In a centrifugation tube, the Au^{3+} solution (2 mM, 1 mL) was mixed with 1 mL of a DDA stock solution (280 mg of DDA dissolved in 10 mL ethanol). After mixing well, it was let stand for more than three hours. 1 mL of degassed toluene was then added to the mixture solution; the light golden yellow toluene solution is on the upper layer. A pipette was used carefully to remove it and bubbled with argon for 10 min, at last, additionally deoxygenated toluene was added to fix it to 1mL (2 M [Au^{3+}] in toluene). Different concentrations of Au^{3+} were made by using different concentrations of $KAuCl_4$ in water using the same process.

Experimental methods in cuvette setup

The DRs samples were diluted in toluene and purged with argon for at least 10 min, to remove the dissolved oxygen in the solution before transfer under argon to a cuvette. The laser exposure area is designed to be circular with a 1 cm-diameter in order to fill a 1 cm wide square cuvette, so the volume of the solution is always kept to 1 cm^3 to be sure that the entire solution volume is exposed to the laser light. The cuvette is then capped under argon, and the solution is continuously stirred at a speed of 300 rpm with a magnetic stirrer. The laser intensity and exposure time are easily adjusted. All the experiments are performed at room temperature.

For dark experiments, the reaction solution is prepared in the dark by mixing as-already made DRs solution and freshly made [Au^{3+}] precursor solution. The order of addition of the reactants to the cuvette is as follows: toluene, DRs in toluene, Au^{3+} in toluene, hole scavenger (MeOH) when needed.

In a typical process: 780 µL toluene, 100 µL DRs in toluene, 20 µL of a 2 mmol/L [Au^{3+}] in toluene, and 100 µL MeOH were mixed under stirring, and then I = 355 mW/cm^2 (P_L = 200 mW) blue laser was applied for 8 min. Then the reaction was stopped by adding 3-fold acetone and purified by centrifugation at 4,000 g, and then redispersed in a chloroform solution.

Control experiments

In order to test the role of each component in the reaction mixture, we carried out several control experiments. i) without MeOH; ii) without laser exposure; iii) without MeOH and laser exposure; iv) without CdSe/CdS semiconductor DRs.

ASSOCIATED CONTENT

Supporting Information

Additional data and figures are included in the Supplementary Information. These data describe: the characterizations of DRs; the optical setup and complementary information on the influence of the concentration of MeOH, the laser intensity, the irradiation time, the gold concentration. This material is available free of charge *via* the Internet at http://pubs.acs.org."

AUTHOR INFORMATION

Corresponding Author

Delville M-H - *CNRS, Univ. Bordeaux, Bordeaux INP, ICMCB, UMR 5026, 87 avenue du Dr. A. Schweitzer, Pessac, F-33608, France.* http://orcid.org/0000-0001-8863-8225 Email: marie-helene.delville@icmcb.cnrs.fr

Delville J-P - *Univ. Bordeaux, CNRS, LOMA, UMR 5798, 33405 Talence, France.* https://orcid.org/0000-0002-7376-9449 Email: jean-pierre.delville@u-bordeaux.fr

Authors

Junjie Hao - *CNRS, Univ. Bordeaux, Bordeaux INP, ICMCB, UMR 5026, 87 avenue du Dr. A. Schweitzer, Pessac, F-33608, France; Univ. Bordeaux, CNRS, LOMA, UMR 5798, 33405 Talence, France.* https://orcid.org/0000-0002-1345-8761.

Haochen Liu - *Department of Electrical and Electronic Engineering, Southern University of Science and Technology, Shenzhen, 518055, China.* https://orcid.org/0000-0002-1801-4879.

Kai Wang - *Department of Electrical and Electronic Engineering, Southern University of Science and Technology, Shenzhen, 518055, China.* https://orcid.org/0000-0003-0443-6955.

Xiaowei Sun - *Department of Electrical and Electronic Engineering, Southern University of Science and Technology, Shenzhen, 518055, China.* https://orcid.org/0000-0002-2840-1880.

Present Addresses

† Junjie Hao present address: *Department of Electrical and Electronic Engineering, Southern University of Science and Technology, Shenzhen, 518055, China.*

Author Contributions

The manuscript was written through contributions of all authors. All authors have given approval to the final version of the manuscript.

Funding Sources

This project has received financial support from the CNRS through the MITI interdisciplinary programs (Action MITI: Nouveaux Matériaux 2020 and 2021), the Ministry of Science and Technology of China (No. 2016YFB0401702 and No.2017YFE0120400), National Natural Science Foundation of China (No. 61674074, 61875082, 61405089, and 62005115), Key-Area Research and Development Program of Guangdong Province (No. 2019B010925001, 2019B010924001), Distinguished Young Scholar of Natural Science Foundation of Guangdong (No. 2017B030306010), Shenzhen Key Laboratory for Advanced Quantum Dot Displays and Lighting (No. ZDSYS201707281632549), Shenzhen Peacock Team Project (No. KQTD2016030111203005).

ACKNOWLEDGMENT

The authors are grateful to Q. Bai (ICMCB, LOMA, CNRS Univ. Bordeaux) and F. Zhao (ICMCB, LOMA, CNRS Univ. Bordeaux) for preliminary discussions. The TEM observations were performed on the microscopes of the Plateforme Aquitaine de Caractérisation des Matériaux (PLACAMAT, UMS 3626, CNRS, Univ. de Bordeaux, Pessac, France). The authors acknowledge Marion Gayot for discussions and help. The HRTEM and STEM were obtained using equipment either at PLACAMAT or at Southern University of Science and Technology Core Research Facilities, and the authors acknowledge the technical support from Dongsheng He and Yang Qiu in SUSTech CRF.

REFERENCES

1. Wu, K.; Zhu, H.; Liu, Z.; Rodríguez-Córdoba, W.; Lian, T., Ultrafast Charge Separation and Long-Lived Charge Separated State in Photocatalytic CdS–Pt Nanorod Heterostructures. *Journal of the American Chemical Society* **2012,** *134*, 10337-10340,

2. Waiskopf, N.; Ben-Shahar, Y.; Galchenko, M.; Carmel, I.; Moshitzky, G.; Soreq, H.; Banin, U., Photocatalytic Reactive Oxygen Species Formation by Semiconductor–Metal Hybrid Nanoparticles. Toward Light-Induced Modulation of Biological Processes. *Nano Lett.* **2016,** *16*, 4266-4273,

3. Khon, E.; Lambright, K.; Khnayzer, R. S.; Moroz, P.; Perera, D.; Butaeva, E.; Lambright, S.; Castellano, F. N.; Zamkov, M., Improving the Catalytic Activity of Semiconductor Nanocrystals through Selective Domain Etching. *Nano Letters* **2013,** *13*, 2016-2023,

4. Nakibli, Y.; Kalisman, P.; Amirav, L., Less Is More: The Case of Metal Cocatalysts. *The Journal of Physical Chemistry Letters* **2015,** *6*, 2265-2268,

5. Chen, Y.; Zhao, S.; Wang, X.; Peng, Q.; Lin, R.; Wang, Y.; Shen, R.; Cao, X.; Zhang, L.; Zhou, G.; Li, J.; Xia, A.; Li, Y., Synergetic Integration of $Cu_{1.94}S–Zn_xCd_{1–x}S$ Heteronanorods for Enhanced Visible-Light-Driven Photocatalytic Hydrogen Production. *Journal of the American Chemical Society* **2016,** *138*, 4286-4289,

6. Regulacio, M. D.; Han, M.-Y., Multinary I-III-VI2 and I2-II-IV-VI4 Semiconductor Nanostructures for Photocatalytic Applications. *Accounts of Chemical Research* **2016,** *49*, 511-519,

7. Ben-Shahar, Y.; Banin, U., Hybrid Semiconductor–Metal Nanorods as Photocatalysts. *Topics in Current Chemistry* **2016,** *374*, 54,

8. Mills, A.; Davies, R. H.; Worsley, D., Water Purification by Semiconductor Photocatalysis. *Chemical Society Reviews* **1993,** *22*, 417-425,

9. Ma, W.; Mao, J.; Hao, C.; Xu, L.; Xu, C.; Kuang, H., Chiral Semiconductor Nanorod Heterostructures with High Photocatalysis Activity. *Applied Catalysis B: Environmental* **2019,** *245*, 691-697,

10. Simon, T.; Carlson, M. T.; Stolarczyk, J. K.; Feldmann, J., Electron Transfer Rate *vs.* Recombination Losses in Photocatalytic H_2 Generation on Pt-Decorated CdS Nanorods. *ACS Energy Letters* **2016,** *1*, 1137-1142,

11. Amirav, L.; Alivisatos, A. P., Photocatalytic Hydrogen Production with Tunable Nanorod Heterostructures. *The Journal of Physical Chemistry Letters* **2010,** *1*, 1051-1054,

12. O'Sullivan, C.; Gunning, R. D.; Barrett, C. A.; Singh, A.; Ryan, K. M., Size Controlled Gold Tip Growth onto II–VI Nanorods. *Journal of Materials Chemistry* **2010,** *20*, 7875-7880,

13. Kusdianto, K.; Jiang, D.; Kubo, M.; Shimada, M., Effect of Annealing Temperature on the Photocatalytic Activity of Ag–TiO_2 Nanocomposite Films by One-Step Gas-Phase Deposition. *Materials Research Bulletin* **2018,** *97*, 497-505,

14. Ozimek, M.; Palewicz, M.; Hreniak, A., Optical Properties of TiO_2 Nanopowder Doped by Silver (Copper) during Synthesis or PVD Method. *Acta Physica Polonica A* **2016,** *129*, 1214-1219,

15. Tang, X.; Kröger, E.; Nielsen, A.; Schneider, S.; Strelow, C.; Mews, A.; Kipp, T., Fluorescent Metal–Semiconductor Hybrid Structures by Ultrasound-Assisted *in Situ* Growth of Gold Nanoparticles on Silica-Coated CdSe-Dot/CdS-Rod Nanocrystals. *Chemistry of Materials* **2019,** *31*, 224-232,

16. Li, J.; Xu, J.; Dai, W.-L.; Fan, K., Dependence of Ag Deposition Methods on the Photocatalytic Activity and Surface State of TiO_2 with Twistlike Helix Structure. *The Journal of Physical Chemistry C* **2009,** *113*, 8343-8349,

17. Pavlopoulos, N. G.; Dubose, J. T.; Hartnett, E. D.; Char, K.; Pyun, J., Colloidal Random Terpolymers: Controlling Reactivity Ratios of Colloidal Comonomers *via* Metal Tipping. *ACS Macro Letters* **2016,** *5*, 950-954,

18. Oros‐Ruiz, S.; Hernández‐Gordillo, A.; García‐Mendoza, C.; Rodríguez‐Rodríguez, A. A.; Gómez, R., Comparative Activity of CdS Nanofibers Superficially Modified by Au, Cu, and Ni Nanoparticles as Co‐Catalysts for Photocatalytic Hydrogen Production under Visible Light. *Journal of Chemical Technology & Biotechnology* **2016,** *91*, 2205-2210,

19. Carbone, L.; Jakab, A.; Khalavka, Y.; Sönnichsen, C., Light-Controlled One-Sided Growth of Large Plasmonic Gold Domains on Quantum Rods Observed on the Single Particle Level. *Nano Letters* **2009,** *9*, 3710-3714,

20. Ben-Shahar, Y.; Scotognella, F.; Kriegel, I.; Moretti, L.; Cerullo, G.; Rabani, E.; Banin, U., Optimal Metal Domain Size for Photocatalysis with Hybrid Semiconductor-Metal Nanorods. *Nature Communications* **2016,** *7*, 10413,

21. Kalisman, P.; Nakibli, Y.; Amirav, L., Perfect Photon-to-Hydrogen Conversion Efficiency. *Nano Letters* **2016,** *16*, 1776-1781,

22. Mokari, T.; Rothenberg, E.; Popov, I.; Costi, R.; Banin, U., Selective Growth of Metal Tips onto Semiconductor Quantum Rods and Tetrapods. *Science* **2004,** *304*, 1787-1790,

23. Saunders, A. E.; Popov, I.; Banin, U., Synthesis of Hybrid CdS−Au Colloidal Nanostructures. *The Journal of Physical Chemistry B* **2006,** *110*, 25421-25429,

24. Mokari, T.; Sztrum, C. G.; Salant, A.; Rabani, E.; Banin, U., Formation of Asymmetric One-Sided Metal-Tipped Semiconductor Nanocrystal Dots and Rods. *Nature Materials* **2005,** *4*, 855,

25. Demortière, A.; Schaller, R. D.; Li, T.; Chattopadhyay, S.; Krylova, G.; Shibata, T.; dos Santos Claro, P. C.; Rowland, C. E.; Miller, J. T.; Cook, R.; Lee, B.; Shevchenko, E. V., *In Situ* Optical and Structural Studies on Photoluminesence Quenching in CdSe/CdS/Au Heterostructures. *Journal of the American Chemical Society* **2014,** *136*, 2342-2350,

26. Menagen, G.; Macdonald, J. E.; Shemesh, Y.; Popov, I.; Banin, U., Au Growth on Semiconductor Nanorods: Photoinduced *versus* Thermal Growth Mechanisms. *Journal of the American Chemical Society* **2009,** *131*, 17406-17411,

27. Menagen, G.; Mocatta, D.; Salant, A.; Popov, I.; Dorfs, D.; Banin, U., Selective Gold Growth on CdSe Seeded CdS Nanorods. *Chemistry of Materials* **2008,** *20*, 6900-6902,

28. Nakibli, Y.; Mazal, Y.; Dubi, Y.; Wächtler, M.; Amirav, L., Size Matters: Cocatalyst Size Effect on Charge Transfer and Photocatalytic Activity. *Nano Letters* **2018,** *18*, 357-364,

29. Dukovic, G.; Merkle, M. G.; Nelson, J. H.; Hughes, S. M.; Alivisatos, A. P., Photodeposition of Pt on Colloidal CdS and CdSe/CdS Semiconductor Nanostructures. *Advanced Materials* **2008,** *20*, 4306-4311,

30. Mongin, D.; Shaviv, E.; Maioli, P.; Crut, A.; Banin, U.; Del Fatti, N.; Vallée, F., Ultrafast Photoinduced Charge Separation in Metal–Semiconductor Nanohybrids. *ACS Nano* **2012,** *6*, 7034-7043,

31. Wenderich, K.; Mul, G., Methods, Mechanism, and Applications of Photodeposition in Photocatalysis: A Review. *Chem. Rev.* **2016,** *116*, 14587-14619,

32. Kenens, B.; Chamtouri, M.; Aubert, R.; Miyakawa, K.; Hayasaka, Y.; Naiki, H.; Watanabe, H.; Inose, T.; Fujita, Y.; Lu, G.; Masuhara, A.; Uji-i, H., Solvent-Induced Improvement of Au Photo-Deposition and Resulting Photo-Catalytic Efficiency of Au/TiO_2. *RSC Advances* **2016,** *6*, 97464-97468,

33. Jiang, Z.; Zhang, Z.; Shangguan, W.; Isaacs, M. A.; Durndell, L. J.; Parlett, C. M. A.; Lee, A. F., Photodeposition as a Facile Route to Tunable Pt Photocatalysts for Hydrogen Production: on the Role of methanol. *Catalysis Science & Technology* **2016,** *6*, 81-88,

34. López, C. R.; Melián, E. P.; Ortega Méndez, J. A.; Santiago, D. E.; Doña Rodríguez, J. M.; González Díaz, O., Comparative Study of Alcohols as Sacrificial Agents in H_2 Production by Heterogeneous Photocatalysis Using Pt/TiO_2 Catalysts. *Journal of Photochemistry and Photobiology A: Chemistry* **2015,** *312*, 45-54,

35. Bai, Q.; Shupyk, I.; Vauriot, L.; Majimel, J.; Labrugere, C.; Delville, M.-H.; Delville, J.-P., Design of Metal@Titanium Oxide Nano-Heterodimers by Laser-Driven Photodeposition: Growth Mechanism and Modeling. *ACS Nano* **2021,** *15*, 2947-2961,

36. Pavlopoulos, N. G.; Dubose, J. T.; Liu, Y.; Huang, X.; Pinna, N.; Willinger, M.-G.; Lian, T.; Char, K.; Pyun, J., Type I *vs.* Quasi-Type II Modulation in CdSe@CdS Tetrapods: Ramifications for Noble Metal Tipping. *CrystEngComm* **2017,** *19*, 6443-6453,

37. Aronovitch, E.; Kalisman, P.; Houben, L.; Amirav, L.; Bar-Sadan, M., Stability of Seeded Rod Photocatalysts: Atomic Scale View. *Chemistry of Materials* **2016,** *28*, 1546-1552,

38. Costi, R.; Saunders, A. E.; Elmalem, E.; Salant, A.; Banin, U., Visible Light-Induced Charge Retention and Photocatalysis with Hybrid CdSe−Au Nanodumbbells. *Nano Letters* **2008,** *8*, 637-641,

39. Pavlopoulos, N. G.; Dubose, J. T.; Pinna, N.; Willinger, M. G.; Char, K.; Pyun, J., Synthesis and Assembly of Dipolar Heterostructured Tetrapods: Colloidal Polymers with “Giant Tert‐Butyl” Groups. *Angewandte Chemie International Edition* **2016,** *55*, 1787-1791,

40. Chakrabortty, S.; Xing, G.; Xu, Y.; Ngiam, S. W.; Mishra, N.; Sum, T. C.; Chan, Y., Engineering Fluorescence in Au-Tipped, CdSe-Seeded CdS Nanoheterostructures. *Small* **2011,** *7*, 2847-2852,

41. Ben-Shahar, Y.; Philbin, J. P.; Scotognella, F.; Ganzer, L.; Cerullo, G.; Rabani, E.; Banin, U., Charge Carrier Dynamics in Photocatalytic Hybrid Semiconductor–Metal Nanorods: Crossover from Auger Recombination to Charge Transfer. *Nano Letters* **2018,** *18*, 5211-5216,

42. Wu, K.; Rodríguez-Córdoba, W. E.; Yang, Y.; Lian, T., Plasmon-Induced Hot Electron Transfer from the Au Tip to CdS Rod in CdS-Au Nanoheterostructures. *Nano Letters* **2013,** *13*, 5255-5263,

43. Singh, R.; Pal, B., Study of Excited Charge Carrier's Lifetime for the Observed Photoluminescence and Photocatalytic Activity of CdS Nanostructures of Different Shapes. *Journal of Molecular Catalysis A: Chemical* **2013,** *371*, 77-85,

44. Volokh, M.; Mokari, T., Metal/Semiconductor Interfaces in Nanoscale Objects: Synthesis, Emerging Properties and Applications of Hybrid Nanostructures. *Nanoscale Advances* **2020,** *2*, 930-961,

45. Khalavka, Y.; Harms, S.; Henkel, A.; Strozyk, M.; Ahijado-Guzmán, R.; Sönnichsen, C., Synthesis of Au–CdS@CdSe Hybrid Nanoparticles with a Highly Reactive Gold Domain. *Langmuir* **2018,** *34*, 187-190,

46. Singh, R.; Pal, B., Influence of Au Photodeposition and Doping in CdS Nanorods: Optical and Photocatalytic Study. *Particulate Science and Technology* **2015,** *33*, 53-58,

47. Yang, J.; Levina, L.; Sargent, E. H.; Kelley, S. O., Heterogeneous Deposition of Noble Metals on Semiconductor Nanoparticles in Organic or Aqueous Solvents. *Journal of Materials Chemistry* **2006,** *16*, 4025-4028,

48. Phillips, K. R.; Jensen, S. C.; Baron, M.; Li, S.-C.; Friend, C. M., Sequential Photo-Oxidation of Methanol to Methyl Formate on TiO_2(110). *Journal of the American Chemical Society* **2013,** *135*, 574-577,

49. Henry, C. R., Growth, Structure and Morphology of Supported Metal Clusters Studied by Surface Science Techniques. *Crystal Research and Technology* **1998,** *33*, 1119-1140,

50. Kominami, H.; Murakami, S.-y.; Kato, J.-i.; Kera, Y.; Ohtani, B., Correlation between Some Physical Properties of Titanium Dioxide Particles and Their Photocatalytic Activity for Some Probe Reactions in Aqueous Systems. *J. Phys. Chem. B* **2002,** *106*, 10501-10507,

51. Mills, A.; O'Rourke, C.; Moore, K., Powder Semiconductor Photocatalysis in Aqueous Solution: An Overview of Kinetics-Based Reaction Mechanisms. *Journal of Photochemistry and Photobiology A: Chemistry* **2015,** *310*, 66-105,

52. Li, J. J.; Wang, Y. A.; Guo, W.; Keay, J. C.; Mishima, T. D.; Johnson, M. B.; Peng, X., Large-Scale Synthesis of Nearly Monodisperse CdSe/CdS Core/Shell Nanocrystals Using Air-Stable

Reagents *via* Successive Ion Layer Adsorption and Reaction. *Journal of the American Chemical Society* **2003,** *125*, 12567-12575,

53. Carbone, L.; Nobile, C.; De Giorgi, M.; Sala, F. D.; Morello, G.; Pompa, P.; Hytch, M.; Snoeck, E.; Fiore, A.; Franchini, I. R.; Nadasan, M.; Silvestre, A. F.; Chiodo, L.; Kudera, S.; Cingolani, R.; Krahne, R.; Manna, L., Synthesis and Micrometer-Scale Assembly of Colloidal CdSe/CdS Nanorods Prepared by a Seeded Growth Approach. *Nano Lett* **2007,** *7*, 2942-2950,

54. Choi, C. L.; Koski, K. J.; Sivasankar, S.; Alivisatos, A. P., Strain-Dependent Photoluminescence Behavior of CdSe/CdS Nanocrystals with Spherical, Linear, and Branched Topologies. *Nano Letters* **2009,** *9*, 3544-3549,

TOC: